Direct Observation and Calipering of the "Webbing" Fermi Surface of Yttrium

S. B. Dugdale, H. M. Fretwell, and M. A. Alam
H.H. Wills Physics Laboratory, University of Bristol,Tyndall Avenue, Bristol, BS8 1TL, United Kingdom

G. Kontrym-Sznajd
Polish Academy of Sciences, W. Trzebiatowski Intsitute of Low Temperature and Structure Research, 50-950 Wrocław 2, P.O. Box 937, Poland

R. N. West and S. Badrzadeh
Department of Physics, University of Texas at Arlington, P.O. Box 19059, Arlington, Texas 76019
(Received 6 January 1997)

The first measurement of both the size and shape of the region of the Fermi surface of yttrium known as the "webbing" is reported. This particular Fermi surface feature is of considerable interest because it is very similar to that found in a number of the heavier rare earth metals, where it is believed to play a vital role in driving the exotic magnetic structures found therein. In this positron study, two-dimensional angular correlation measurements combined with three-dimensional reconstruction provide a direct image of this part of the yttrium Fermi surface. [S0031-9007(97)03771-X]

PACS numbers: 78.70.Bj, 71.18.+y, 71.20.–b, 87.59.Fm

Many of the heavier rare earths (e.g., Tb, Dy, Ho, Er) display a helical antiferromagnetic ordering, where the localized $4f$ moments are coupled via the Ruderman-Kittel-Kasuya-Yosida indirect exchange interaction involving the conduction electrons [1]. The ability of the conduction electrons to establish magnetic order depends strongly on the Fermi surface (FS) topology [2]. That dependence is most easily understood in terms of the wave-vector dependent susceptibility,

$$\chi(\mathbf{q}) \propto \sum_{\mathbf{k},j,j'} \frac{|M(\mathbf{k},\mathbf{k}+\mathbf{q})|^2 f_{kj}(1-f_{k+q+Gj'})}{\epsilon_{j'}(\mathbf{k}+\mathbf{q}+\mathbf{G})-\epsilon_j(\mathbf{k})}. \quad (1)$$

Here M is a matrix element involving the wave functions of the conduction electrons and the localized f electrons, the f_{kj} is the Fermi-Dirac distribution function for reduced wave vector $\mathbf{k}$ and band j, the $\epsilon_j(\mathbf{k})$ are the single particle energies, and $\mathbf{G}$ is the reciprocal lattice vector that brings $\mathbf{k}+\mathbf{q}$ back into the first Brillouin zone (BZ). Subject to other constraints [1], the maximum in $\chi(\mathbf{q})$ determines the $\mathbf{q}$ vector of the most stable magnetic configuration. If the maximum of $\chi(\mathbf{q})$ is at $\mathbf{q}=0$, the material will be ferromagnetic. If it is at some other $\mathbf{q}$, a more complex arrangement of spins will ensue, with a wavelength defined by that vector. The latter condition may well occur when there are large parallel sections of Fermi surface and an appreciable "weight" of the terms in Eq. (1) have vanishingly small denominators at the "spanning" or "nesting" vector. It is a so-called "webbing" feature [3,4] in the Fermi surface of some of the rare earths which provides large parallel FS sheets for a nesting that drives the magnetic ordering.

A paucity of high-quality samples of the heavy rare earths has hindered direct investigations of the intimate relationship between FS topology and magnetic behavior in these systems. The interest in the more easily refined $4d$ transition metal yttrium (Y) arises from the fact that its FS is predicted to possess a similar and strong webbing feature [3] (even though the lack of local moments excludes magnetic ordering). However, if alloyed with the heavier rare earths, the combination of the local moments of the rare earths and the strong nesting properties of the yttrium FS might result in magnetic ordering at the appropriate $\mathbf{q}$, and thereby provide a direct test of the concept of FS-driven ordering. This is not a new idea. Long-range magnetic ordering in gadolinium-yttrium superstructures has been explained in terms of the Fermi surface topology of the nonmagnetic Y layers [5]. An obvious prerequisite for further studies is a direct elucidation of the webbing feature and associated large parallel Fermi surface sheets in Y.

Figure 1 shows the Fermi surface of Y as determined by an augmented plane wave calculation performed by Loucks [3] (subsequent self-consistent calculations, such as that of Skriver and Mackintosh [6], have yielded very similar Fermi surface topologies). Shown in the double zone scheme, the Fermi surface is in bands 3 and 4 (which, in the absence of spin-orbit coupling, are degenerate on the *A-L-H* plane). The webbing, identifiable as the flat areas in both bands on either side of the *A-L-H* plane, has a nesting vector, denoted in Fig. 1 by $\mathbf{Q}_0$. This vector has been related to the wave vector associated with the exotic magnetic structures [2]. Although de Haas–van Alphen (dHvA) experiments [4,7] have provided evidence for the existence of a Fermi surface which exhibits this feature, such efforts deliver only *extremal* Fermi surface areas. In this Letter, we present the first glimpse of both the shape and size of this webbing, uniquely (and directly) obtained by the positron annihilation method.

For many years, positron annihilation experiments have made significant contributions to our understanding of

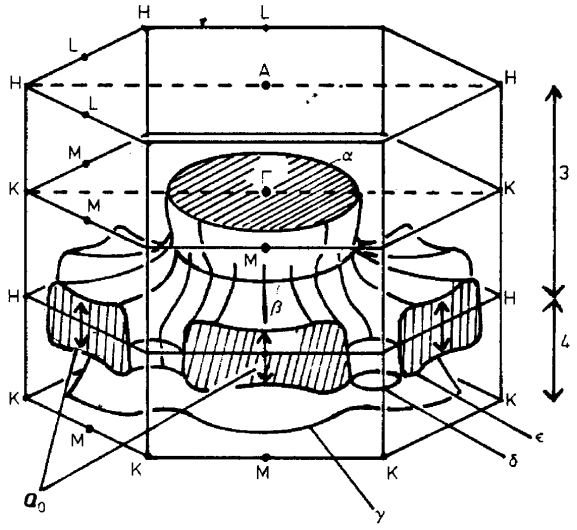

FIG. 1. The third and fourth band Fermi surface sheets of Y, proposed by Loucks [3] and reproduced from Mattocks and Young [4]. The labels (e.g., α) denote some of the dHvA frequencies and the magnetic vector $\mathbf{Q_0}$; linking the webbing from the two bands is shown.

the electronic structure of metals [8]. When a thermal positron annihilates with an electron in a solid sample, there is some small (~mrad) deviation from anticollinearity of the two photons arising from the finite momentum of the electron in the laboratory frame. By measuring the angular distribution of these deviations, one can derive information directly related to the momentum of the electron in the sample immediately before annihilation. The conventional two-dimensional angular correlation of positron annihilation radiation (2D-ACAR) measurement yields a 2D projection (or integral over one dimension), $N(p_x, p_y)$, of the two-photon momentum density, $\rho^{2\gamma}(\mathbf{p})$. Within the independent particle model,

$$\rho^{2\gamma}(\mathbf{p}) = \sum_k \sum_{\text{occ.}} \left| \int d\mathbf{r}\, \psi_{k,j}(\mathbf{r})\psi_+(\mathbf{r}) \exp(-i\mathbf{p}\cdot\mathbf{r}) \right|^2 = \sum_{j,\mathbf{k},\mathbf{G}} n^j(\mathbf{k}) |C_{\mathbf{G},j}(\mathbf{k})|^2 \delta(\mathbf{p} - \mathbf{k} - \mathbf{G}), \quad (2)$$

where $\psi_{k,j}(\mathbf{r})$ and $\psi_+(\mathbf{r})$ are the electron and positron wave functions, respectively, j is a band index, $\mathbf{G}$ is a reciprocal lattice vector, and $n^j(\mathbf{k})$ is the electron occupancy in $\mathbf{k}$ space associated with band j. The $C_{\mathbf{G},j}(\mathbf{k})$ are the Fourier coefficients of the electron-positron wavefunction product. The delta function expresses the conservation of (crystal) momentum. It may be seen that $\rho^{2\gamma}(\mathbf{p})$ contains information about the occupied electron states of the system and their momentum, $\mathbf{p} = \hbar(\mathbf{k} + \mathbf{G})$. Most significantly, in the case of a metal, whenever a partially occupied band crosses the Fermi level, there is a discontinuity in $\rho^{2\gamma}(\mathbf{p})$ at a number of points, $\mathbf{p}_F = \hbar(\mathbf{k}_F + G)$. The 2D-ACAR spectra, as already noted above, represent projections of $\rho^{2\gamma}(\mathbf{p})$, but if one measures a small number of projections, with integrations along different crystallographic directions, it is possible to reconstruct $\rho^{2\gamma}(\mathbf{p})$ [8]. Finally, if this 3D density is folded back into the first BZ [9] [and the effects of the positron wave function are assumed to be small so that the $C_{\mathbf{G},j}(\mathbf{k})$ are essentially independent of $\mathbf{k}$], the translational invariance is restored and an electron occupancy in $\mathbf{k}$ space, $n^j(\mathbf{k})$, is obtained,

$$n(\mathbf{k}) = \sum_{\mathbf{G}} \rho^{2\gamma}(\mathbf{k} + \mathbf{G}), \quad (3)$$

where $\mathbf{G}$ is the reciprocal lattice vector necessary to bring $\mathbf{p}[= \hbar(\mathbf{k} + \mathbf{G})]$ back into the first BZ. By these means, one can directly "image" the Fermi surface in the reconstructed 3D spectra [10].

In these experiments, five projections were measured at 7.5° intervals, encompassing the 30° between the directions Γ-M and Γ-K (in the unique segment of the BZ) on a single crystal specimen of Y, using the 2D-ACAR spectrometer at the University of Texas at Arlington. For technical reasons, the experiments were performed at room temperature, with an overall resolution of approximately 0.15 atomic units (a.u.) of momentum. Following the usual processing of the measured spectra [8], a "Maximum Entropy" (MaxEnt)-based deconvolution procedure was also applied to each spectrum to suppress the unwanted smearing introduced by the experimental resolution [11]. The strength of the MaxEnt method is that it does not introduce artifacts into the data. The benefit of applying this procedure before reconstruction, in respect to the quality of the resulting 3D momentum densities, was demonstrated by Fretwell *et al.* [12].

Techniques for reconstructing a function from its linear projections are often borrowed from medical tomography. However, reconstruction from just a few measured projections requires exploitation of the crystallographic symmetry. Here, the full 3D $\rho^{2\gamma}(\mathbf{p})$ was reconstructed from the five measured spectra (both "raw" and MaxEnt deconvoluted) using Cormack's method [13–15], before finally following the Lock-Crisp-West prescription [9] to fold the momentum distribution back into the first BZ. The two reconstructions derived from the undeconvoluted and deconvoluted projections will be referred to as raw and "MaxEnt," respectively. The reconstruction procedure itself was rigorously tested [15], and was again shown not to introduce artifacts into the data. A more detailed description of these procedures can be found in Dugdale [16], and a full report is currently in preparation [17].

As noted earlier, the final result of the angular correlation experiments is an electron occupancy (or density) including both fully and partially occupied bands. But, by using a threshold criterion to differentiate between empty and occupied states (and here that proved easy to do), it is possible to image the occupied bands and the Fermi surface alone [10]. Figure 2 shows an image of the Fermi surface of Y, obtained from the MaxEnt-deconvoluted projections. The image obtained from the raw reconstruction (not shown) is similar, but, not unexpectedly, the

FIG. 2. The Fermi surface of Y obtained from the positron annihilation experiment. The webbing can clearly be identified as the flat areas in the *A-L-H* plane (see Fig. 1). Note the similarity to the band 3 surface of Fig. 1.

structures are less sharp. In a multiband system, and particularly when positron effects are present, one might expect it to be difficult to clearly resolve the Fermi surface sheets associated with each individual band. Figure 2, however, shows remarkable similarity with the band 3 Fermi surface of Loucks (Fig. 1), clearly exposing the extensive flat areas which comprise the webbing. The assertion that the webbing is a relatively flat area of Fermi surface close to the *A-L-H* plane can therefore be confirmed. Furthermore, the dHvA experiments of Mattocks and Young [4] suggested that the webbing was an area where the density of states was large, which would further enhance any nesting phenomenon.

One may examine the webbing in greater detail. Figure 3 shows the section through the webbing in the *H-L-M-K* plane (i.e., on the face of the BZ) that results from the MaxEnt reconstruction. In this figure, the lows (holes) are shown as black, and the highs (electrons) as white. The webbing can be identified as the central black region of holes. If now the raw and MaxEnt reconstructions are normalized so that they contain the same number of "electrons" within the BZ, and the raw reconstruction is subtracted from the MaxEnt reconstruction, the distribution shown in Fig. 4 results. This procedure amounts to an "edge-enhancement" or high-frequency filter technique which previously has been shown to highlight Fermi surface features [11]. It enhances the edges or discontinuities because it is in the vicinity of those discontinuities in the occupation density that the resolution function has had the most damaging effect. Thus by subtracting the raw from the "enhanced" distribution, one is, in essence, amplifying the Fermi surface information. Figure 5 displays the "zero" contour, and therein is a striking resemblance between the theoretical prediction (Fig. 1) and this contour, i.e., the contour where the difference between the two distributions is zero defines the Fermi surface.

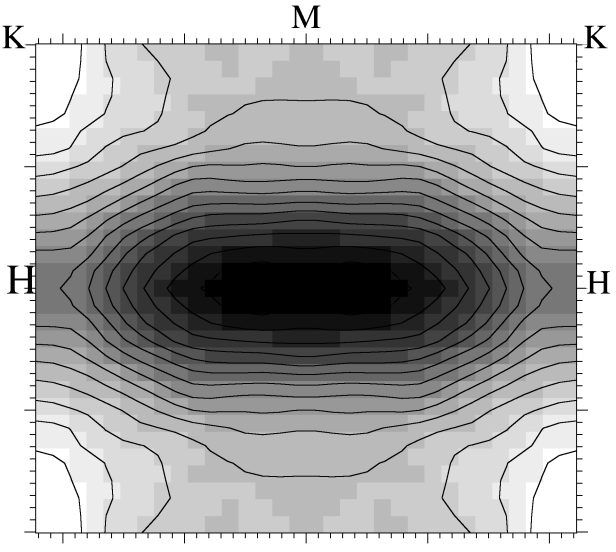

FIG. 3. Experimental cross sections, in the *H-L-M-K* plane, showing the webbing, from the MaxEnt reconstruction. The labels indicate the BZ symmetry points.

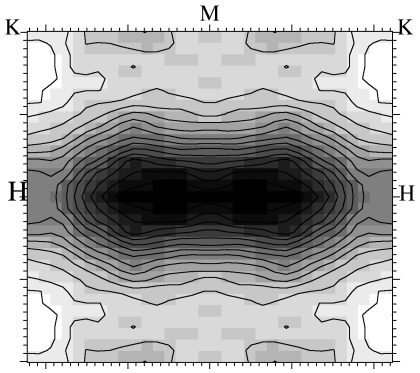

FIG. 4. Experimental cross section, in the *H-L-M-K* plane, obtained by constructing the difference between the MaxEnt and raw reconstructions. The labels indicate the BZ symmetry points.

With this technique, it is possible to caliper the width of the webbing in the direction *M-L-M*. In Fig. 6, a section along this direction through the difference spectrum (Fig. 4) is plotted. It was proposed by Dugdale *et al.* [11]

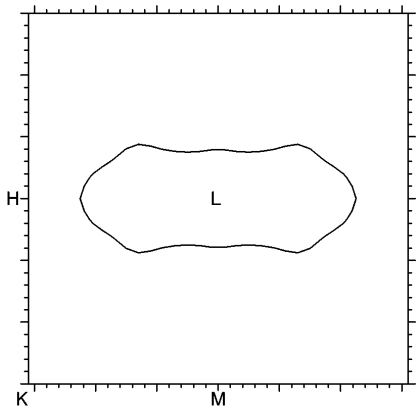

FIG. 5. The webbing Fermi surface of Y, obtained by plotting the zero contour of the difference distribution of Fig. 4.

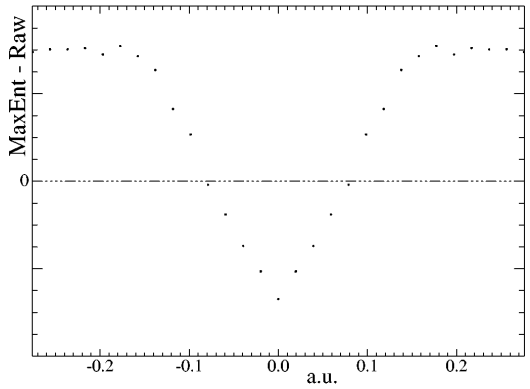

FIG. 6. Cut in the *M-L-M* direction through the distribution of Fig. 4, used to caliper the Fermi surface, by finding the locations where this distribution passes through zero.

that the locations where such a difference distribution passes through zero ought to define the Fermi surface. This immediately suggests a method for calipering the Fermi surface, based upon measuring the distance between these zero crossings. In this way, the width of the webbing, and hence the magnitude of the magnetic **Q** vector, was found to be $(0.55 \pm 0.02) \times (\frac{\pi}{c})$. Although pure Y is paramagnetic, by alloying with a small amount of terbium, spiral magnetic structures do appear with a typical **Q** of magnitude $0.56 \times (\frac{\pi}{c})$ [18,19]. Caudron *et al.* [20] performed neutron experiments on alloys of Y with less than 0.5 at. % erbium, observing long-range order with a period of $(0.54 \pm 0.02) \times (\frac{\pi}{c})$, even at a concentration of only 0.5 at. %. Vinkurova *et al.* [7] performed dHvA experiments on Y, and inferred a vector **Q** of magnitude $0.58 \times (\frac{\pi}{c})$ (no error stated) from the webbing. In view of this, the current caliper is in excellent agreement with others' measurements.

Finally, it is also possible to make contact with the dHvA results of Mattocks and Young [4], by calculating the cross-sectional area of the webbing in the *H-L-M-K* plane. This was achieved by measuring the area where the difference was negative. The area was found to be (0.071 ± 0.004) a.u.^{2}, in comparison with the dHvA value of (0.0759 ± 0.0008) a.u.^{2} (taken from the band 4 ϵ_3 orbit from [4]). Since this is likely to be some average of the band 4 and band 3 orbits (the orbit associated with band 3 is 0.05747 ± 0.00006 a.u.^{2}), the agreement can be considered even better.

In conclusion, the existence of flat areas of Fermi surface in the vicinity of the *A-L-H* plane has been confirmed by directly imaging the Fermi surface. These flat areas are ideal for supporting Fermi surface nesting, which is thought to drive the exotic magnetic structures found in many of the heavier rare earths. Precise and unique quantitative information about the shape and size webbing was obtained.

The authors would like to acknowledge the EPSRC and the Royal Society (UK) and the State Committee for Scientific Research (Republic of Poland) (Grant No. 2 P302 161 06) for their financial support. One of us (S.B.D.) would like to thank the Foundation Governors of CRGS (UK) for generously financing travel.

[1] T. Kasuya, in *Magnetism*, edited by G. T. Rado and H. Suhl (Academic Press Inc., New York, 1966), Vol. IIB, p. 215.
[2] W. E. Evenson and S. H. Liu, Phys. Rev. **178**, 783 (1969).
[3] T. L. Loucks, Phys. Rev. **144**, 504 (1966).
[4] P. G. Mattocks and R. C. Young, J. Phys. F **8**, 1417 (1978).
[5] C. F. Majkrzak *et al.*, J. Appl. Phys. **61**, 4055 (1987).
[6] H. L. Skriver and A. R. Mackintosh, in *Physics of Transition Metals* (Inst. Phys. Conf. Series, Bristol, 1980), No. 55, p. 29.
[7] L. I. Vinokurova *et al.*, JETP Lett. **34**, 566 (1981).
[8] R. N. West, in *Proceedings of the International School of Physics "Enrico Fermi"—Positron Spectroscopy of Solids*, edited by A. Dupasquier and A. P. Mills, Jr. (IOS Press, Amsterdam, 1995).
[9] D. G. Lock, V. H. C. Crisp, and R. N. West, J. Phys. F **3**, 561 (1973).
[10] A. A. Manuel, Phys. Rev. Lett. **49**, 1525 (1982).
[11] S. B. Dugdale *et al.*, J. Phys. Condens. Matter **6**, L435 (1994).
[12] H. M. Fretwell *et al.*, Europhys. Lett. **32**, 771 (1995).
[13] A. M. Cormack, J. Appl. Phys. **34**, 2722 (1963).
[14] A. M. Cormack, J. Appl. Phys. **35**, 2908 (1964).
[15] G. Kontrym-Sznajd, Phys. Status Solidi (a) **117**, 227 (1990).
[16] S. B. Dugdale, Ph.D. thesis, University of Bristol, 1996 (unpublished).
[17] G. Kontrym-Sznajd, S. B. Dugdale, H. M. Fretwell, M. A. Alam, R. N. West, and S. Badrzadeh (to be published).
[18] H. R. Child and W. C. Koehler, Phys. Rev. **174**, 562 (1968).
[19] N. Wakabayashi and R. M. Nicklow, Phys. Rev. B **10**, 2049 (1974).
[20] R. Caudron *et al.*, Phys. Rev. B **42**, 2325 (1990).